PROCEEDINGS OF SPIE

SPIEDigitalLibrary.org/conference-proceedings-of-spie

QUBIC: the Q and U bolometric interferometer for cosmology

C. O'Sullivan, P. Ade, G. Amico, D. Auguste, J. Aumont, et al.

C. O'Sullivan, P. Ade, G. Amico, D. Auguste, J. Aumont, S. Banfi, G. Barbarán, P. Battaglia, E. Battistelli, A. Baù, B. Bélier, D. Bennett, L. Bergé, J.-Ph. Bernard, M. Bersanelli, M.-A. Bigot-Sazy, N. Bleurvacq, J. Bonaparte, J. Bonis, G. Bordier, E. Bréelle, E. Bunn, D. Burke, D. Buzi, A. Buzzelli, F. Cavaliere, P. Chanial, C. Chapron, R. Charlassier, F. Columbro, G. Coppi, A. Coppolecchia, F. Couchot, R. D'Agostino, G. D'Alessandro, P. de Bernardis, G. de Gasperis, M. De Leo, M. De Petris, A. Di Donato, L. Dumoulin, A. Etchegoyen, A. Fasciszewski, C. Franceschet, M. M. Gamboa Lerena, B. García, X. Garrido, M. Gaspard, A. Gault, D. Gayer, M. Gervasi, M. Giard, Y. Giraud-Héraud, M. Gómez Berisso, M. González, M. Gradziel, L. Grandsire, E. Guerrard, J.-Ch. Hamilton, D. Harari, V. Haynes, S. Henrot-Versillé, D. T. Hoang, F. Incardona, E. Jules, J. Kaplan, A. Korotkov, C. Kristukat, L. Lamagna, S. Loucatos, T. Louis, A. Lowitz, V. Lukovic, R. Luterstein, B. Maffei, S. Marnieros, S. Masi, A. Mattei, A. May, M. McCulloch, M. C. Medina, L. Mele, S. Melhuish, A. Mennella, L. Montier, L. M. Mundo, J. A. Murphy, J. D. Murphy, E. Olivieri, A. Paiella, F. Pajot, A. Passerini, H. Pastoriza, A. Pelosi, C. Perbost, O. Perdereau, F. Pezzotta, F. Piacentini, M. Piat, L. Piccirillo, G. Pisano, G. Polenta, D. Prêle, R. Puddu, D. Rambaud, P. Ringegni, G. E. Romero, M. Salatino, A. Schillaci, C. G. Scóccola, S. Scully, S. Spinelli, M. Stolpovskiy, F. Suarez, A. Tartari, J.-P. Thermeau, P. Timbie, S. A. Torchinsky, M. Tristram, V. Truongcanh, C. Tucker, G. Tucker, S. Vanneste, D. Viganò, N. Vittorio, F. Voisin, B. Watson, F. Wicek, M. Zannoni, A. Zullo, "QUBIC: the Q and U bolometric interferometer for cosmology," Proc. SPIE 10708, Millimeter, Submillimeter, and Far-Infrared Detectors and Instrumentation for Astronomy IX, 107082B (9 July 2018); doi: 10.1117/12.2313332

SPIE.

Event: SPIE Astronomical Telescopes + Instrumentation, 2018, Austin, Texas, United States

Downloaded From: https://www.spiedigitallibrary.org/conference-proceedings-of-spie on 12/20/2018 Terms of Use: https://www.spiedigitallibrary.org/terms-of-use

QUBIC: the Q and U bolometric interferometer for cosmology

C. O'Sullivan*[a], P. Ade[b], G. Amico[c], D. Auguste[d], J. Aumont[e], S. Banfi[f,g], G. Barbarán[h], P. Battaglia[i], E. Battistelli[c,j], A. Baù[f,g], B. Bélier[k], D. Bennett[a], L. Bergé[l], J.-Ph. Bernard[m], M. Bersanelli[i,n], M.-A. Bigot-Sazy[o], N. Bleurvacq[o], J. Bonaparte[p], J. Bonis[d], G. Bordier[o], E. Bréelle[o], E. Bunn[q], D. Burke[a], D. Buzi[c], A. Buzzelli[r], F. Cavaliere[i], P. Chanial[o], C. Chapron[o], R. Charlassier[o], F. Columbro[c], G. Coppi[s], A. Coppolecchia[c,j], F. Couchot[d], R. D'Agostino[r], G. D'Alessandro[c,j], P. de Bernardis[c, j], G. De Gasperis[r], M. De Leo[c], M. De Petris[cj], A. Di Donato[p], L. Dumoulin[l], A. Etchegoyen[t], A. Fasciszewski[p], C. Franceschet[i,n], M. M. Gamboa Lerena[u], B. García[t], X. Garrido[d], M. Gaspard[d], A. Gault[v], D. Gayer[a], M. Gervasi[f,g], M. Giard[m], Y. Giraud-Héraud[o], M. Gómez Berisso[w], M. González[w], M. Gradziel[a], L. Grandsire[o], E. Guerrard[d], J.-Ch. Hamilton[o], D. Harari[w], V. Haynes[s], S. Henrot-Versillé[d], D. T. Hoang[o], F. Incardona[i,n], E. Jules[d], J. Kaplan[o], A. Korotkov[x], C. Kristukat[y], L. Lamagna[c, j], S. Loucatos[o], T. Louis[d], A. Lowitz[v], V. Lukovic[r], R. Luterstein[h], B. Maffei[e], S. Marnieros[l], S. Masi[c, j], A. Mattei[j], A. May[s], M. McCulloch[s], M.C. Medina[z], L. Mele[c], S. Melhuish[s], A. Mennella[i,n], L. Montier[m], L. M. Mundo[aa], J.A. Murphy[a], J.D. Murphy[a], E. Olivieri[l], A. Paiella[c, j], F. Pajot[m], A. Passerini[f,g], H. Pastoriza[w], A. Pelosi[j], C. Perbost[o], O. Perdereau[d], F. Pezzotta[i], F. Piacentini[c, j], M. Piat[o], L. Piccirillo[s], G. Pisano[b], G. Polenta[c, j], D. Prêle[o], R. Puddu[c, j], D. Rambaud[m], P. Ringegni[aa], G. E. Romero[z], M. Salatino[o], A. Schillaci[ab], C. G. Scóccola[u], S. Scully[a,ac], S. Spinelli[f], M. Stolpovskiy[o], F. Suarez[t], A. Tartari[o], J.-P. Thermeau[o], P. Timbie[v], S.A. Torchinsky[o], M. Tristram[d], V. Truongcanh[d], C. Tucker[b], G. Tucker[x], S. Vanneste[d], D. Viganò[i], N. Vittorio[r], F. Voisin[o], B. Watson[s], F. Wicek[d], M. Zannoni[f,g], A. Zullo[j].

[a]Dept. of Exp. Physics, National University of Ireland, Maynooth, Co. Kildare, Ireland; [b]School of Physics and Astronomy, Cardiff University, UK; [c]Dip. Fisica, Università di Roma "La Sapienza", Roma, Italy; [d]Laboratoire de l'Accélérateur Linéaire (CNRS-IN2P3), Orsay, Paris, France; [e]Institut d'Astrophysique Spatiale (CNRS-INSU), Orsay, Paris, France; [f]Physics Department, Università di Milano – Bicocca, Milano, Italy; [g]INFN Milano-Bicocca, Milano, Italy; [h]Regional Noroeste (CNEA), Salta City, Salta Province, Argentina; [i]Physics Department, Università degli Studi di Milano, Milano, Italy; [j]INFN, Sezione di Roma 1, Roma, Italy; [k]Centre de Nanosciences et de Nanotechnologies, Orsay, Paris, France; [l]Centre de Spectrométrie Nucléaire et de Spectrométrie de Masse (CNRS-IN2P3), Orsay, Paris, France; [m]Institut de Recherche en Astrophysique et Planétologie (CNRS-INSU), Toulouse, France; [n]INFN Milano, Milano, Italy; [o]Astroparticule et Cosmologie (CNRS-IN2P3), Université Paris Diderot-Paris 7, France; [p]Centro Atómico Constituyentes (CNEA), Buenos Aires, Argentina; [q]University of Richmond, Richmond, VA, USA; [r]Università di Roma – Tor Vergata, Roma, Italy; [s]School of Physics & Astronomy, University of Manchester, UK; [t]Instituto de Tecnologías en Detección y Astropartículas (CNEA, CONICET, UNSAM), Buenos Aires, Argentina; [u]Facultad de Cs Astronómicas y Geofísicas (FCAG-UNLP/CONICET), Universidad Nacional de La Plata, Argentina; [v]University of Wisconsin, Madison, WI, USA; [w]Centro Atómico Bariloche and Instituto Balseiro (CNEA), Río Negro, Argentina; [x]Brown University, Providence, RI, USA; [y]Escuela de Ciencia y Tecnología (UNSAM), Buenos Aires, Argentina; [z]Instituto Argentino de Radioastronomía (CONICET, CIC), Buenos Aires, Argentina; [aa]GEMA, Universidad Nacional de La Plata, Buenos Aires, Argentina; [ab]California Institute of Technology (Caltech), Pasadena, CA 91125, USA; [ac]Institute of Technology Carlow, Co. Carlow, Ireland

*corresponding author: creidhe.osullivan@mu.ie

Millimeter, Submillimeter, and Far-Infrared Detectors and Instrumentation for Astronomy IX,
edited by Jonas Zmuidzinas, Jian-Rong Gao, Proc. of SPIE Vol. 10708, 107082B
© 2018 SPIE · CCC code: 0277-786X/18/$18 · doi: 10.1117/12.2313332

Downloaded From: https://www.spiedigitallibrary.org/conference-proceedings-of-spie on 12/20/2018
Terms of Use: https://www.spiedigitallibrary.org/terms-of-use

ABSTRACT

QUBIC, the Q & U Bolometric Interferometer for Cosmology, is a novel ground-based instrument that has been designed to measure the extremely faint B-mode polarisation anisotropy of the cosmic microwave background at intermediate angular scales (multipoles of $l = 30 - 200$). Primordial B-modes are a key prediction of Inflation as they can only be produced by gravitational waves in the very early universe. To achieve this goal, QUBIC will use bolometric interferometry, a technique that combines the sensitivity of an imager with the systematic error control of an interferometer. It will directly observe the sky through an array of 400 back-to-back entry horns whose signals will be superimposed using a quasi-optical beam combiner. The resulting interference fringes will be imaged at 150 and 220 GHz on two focal planes, each tiled with NbSi Transition Edge Sensors, cooled to 320 mK and read out with time-domain multiplexing. A dichroic filter placed between the optical combiner and the focal planes will select the two frequency bands. A very large receiver cryostat will cool the optical and detector stages to 40 K, 4 K, 1 K and 320 mK using two pulse tube coolers, a novel 4He sorption cooler and a double-stage 3He/4He sorption cooler. Polarisation modulation and selection will be achieved using a cold stepped half-wave plate (HWP) and polariser, respectively, in front of the sky-facing horns. A key feature of QUBIC's ability to control systematic effects is its 'self-calibration' mode where fringe patterns from individual equivalent baselines can be compared. When observing, however, all the horns will be open simultaneously and we will recover a synthetic image of the sky in the I, Q and U Stokes' parameters. The synthesised beam pattern has a central peak of approximately 0.5 degrees in width, with secondary peaks further out that are damped by the 13-degree primary beam of the horns. This is Module 1 of QUBIC which will be installed in Argentina, near the city of San Antonio de los Cobres, at the Alto Chorrillos site (4869 m a.s.l.), Salta Province. Simulations have shown that this first module could constrain the tensor-to-scalar ratio down to $\sigma(r) = 0.01$ after a two-year survey. We aim to add further modules in the future to increase the angular sensitivity and resolution of the instrument.

The QUBIC project is proceeding through a sequence of steps. After an initial successful characterisation of the detection chain, a technological demonstrator is being assembled to validate the full instrument design and to test it electrically, thermally and optically. The technical demonstrator is a scaled-down version of Module 1 in terms of the number of detectors, input horns and pulse tubes and a reduction in the diameter of the combiner mirrors and filters, but is otherwise similar. The demonstrator will be upgraded to the full module in 2019. In this paper we give an overview of the QUBIC project and instrument.

Keywords: CMB, B-modes, bolometric interferometry, QUBIC

1. INTRODUCTION

1.1. Polarisation anisotropies in the CMB

The cosmic microwave background (CMB) is a background of thermal radiation left from an early hot dense phase of the Universe. Structure formation in this early Universe left faint temperature and polarisation imprints[1] in the otherwise uniform background and the observation of these over the past two decades has led to a remarkable increase in our understanding of cosmology. To-date, all observations are consistent with the so-called ΛCDM standard cosmological model with a period of accelerated expansion, known as Inflation, required to account for some properties without the need for fine tuning initial conditions.

The temperature anisotropy in the CMB has been mapped with exquisite sensitivity by ESA's Planck satellite[2]. Polarisation anisotropies are at a much lower level and are usually decomposed into their E-mode (curl-free) and B-mode (divergence-free) components. Structure formation gave rise to the dominant E-mode polarisation anisotropy whereas gravitational waves, if they existed, would have given rise to extremely faint B-modes. Gravitational waves, and therefore primordial B-modes, are a key prediction of Inflation[3] but have yet to be detected. (B-modes arising from the lensing of E-modes by intervening large-scale structure in the Universe have, on the other hand.) Unfortunately, B-modes must be measured against a strong foreground of instrumental, atmospheric and galactic sources of polarisation which are themselves unknown in many cases.

The exact level of the primordial B-modes depends strongly on the energy scale of Inflation and is unknown. It is usually described in terms of the tensor-to-scalar ratio, r, that compares the level of the B-modes with that of the E-modes. ESA's

Downloaded From: https://www.spiedigitallibrary.org/conference-proceedings-of-spie on 12/20/2018
Terms of Use: https://www.spiedigitallibrary.org/terms-of-use

Planck mission has placed an upper bound on this ratio of $r_{0.002} < 0.11$ (95% CL), consistent with a B-mode polarisation constraint $r_{0.05} < 0.07$ (95% CL) obtained from a joint BICEP2/Keck Array and Planck analysis[4]. The simplest inflationary models predict $r > 0.01$.

1.2 QUBIC

The Q & U Bolometric Interferometer for Cosmology (QUBIC)[5,6], is a novel ground-based instrument designed to measure the extremely faint primordial B-mode polarisation anisotropies of the CMB, at multipoles in the range $l = 30 - 200$, using the novel technique of bolometric interferometry. A key feature of QUBIC is its ability to control systematic effects by comparing fringe patterns from individual equivalent baselines[7,8] (Figure 1). The QUBIC module will observe the sky in two frequency bands (centred on 150 GHz and 220 GHz, for foreground removal) from a site in Argentina and simulations have shown that it could constrain the tensor-to-scalar ratio down to $\sigma(r) = 0.01$ after a two-year survey[9]. Further modules could be added in the future to increase the angular sensitivity and resolution of the instrument. The QUBIC collaboration now has more than 100 members from 6 countries.

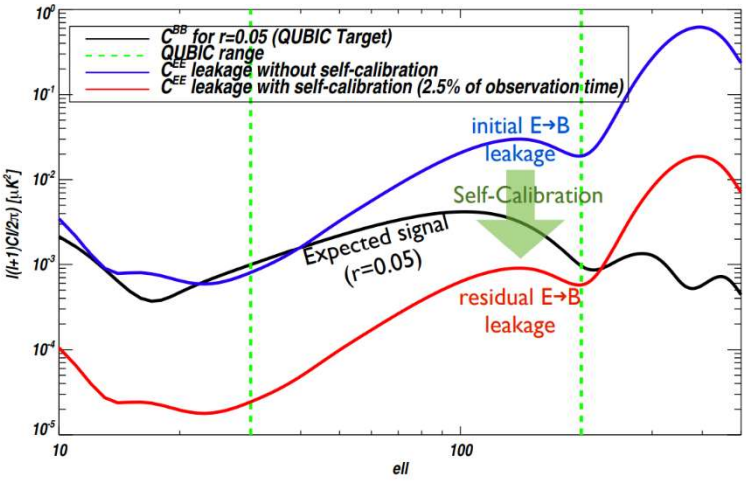

Figure 1. The improvement in achievable sensitivity to the CMB B-mode signal if QUBIC self-calibration is used[6].

1.3 Layout of the paper

Section 2 explains the concept behind the operation of the QUBIC instrument before its individual subsections are described in more detail in Section 3. We finish by discussing the QUBIC technical demonstrator, currently undergoing integration and testing in France.

2. THE QUBIC CONCEPT

QUBIC operates as a Fizeau interferometer, superimposing the beams from an array of 400 back-to-back horns at its entrance aperture onto a focal plane. Each pair of horns produces the image of a fringe pattern which is then sampled by an array of bolometers, hence we use the term *bolometric interferometry*. A schematic diagram of QUBIC is shown in Figure 2. Note that the optical chain is completely contained within the cryostat.

Downloaded From: https://www.spiedigitallibrary.org/conference-proceedings-of-spie on 12/20/2018
Terms of Use: https://www.spiedigitallibrary.org/terms-of-use

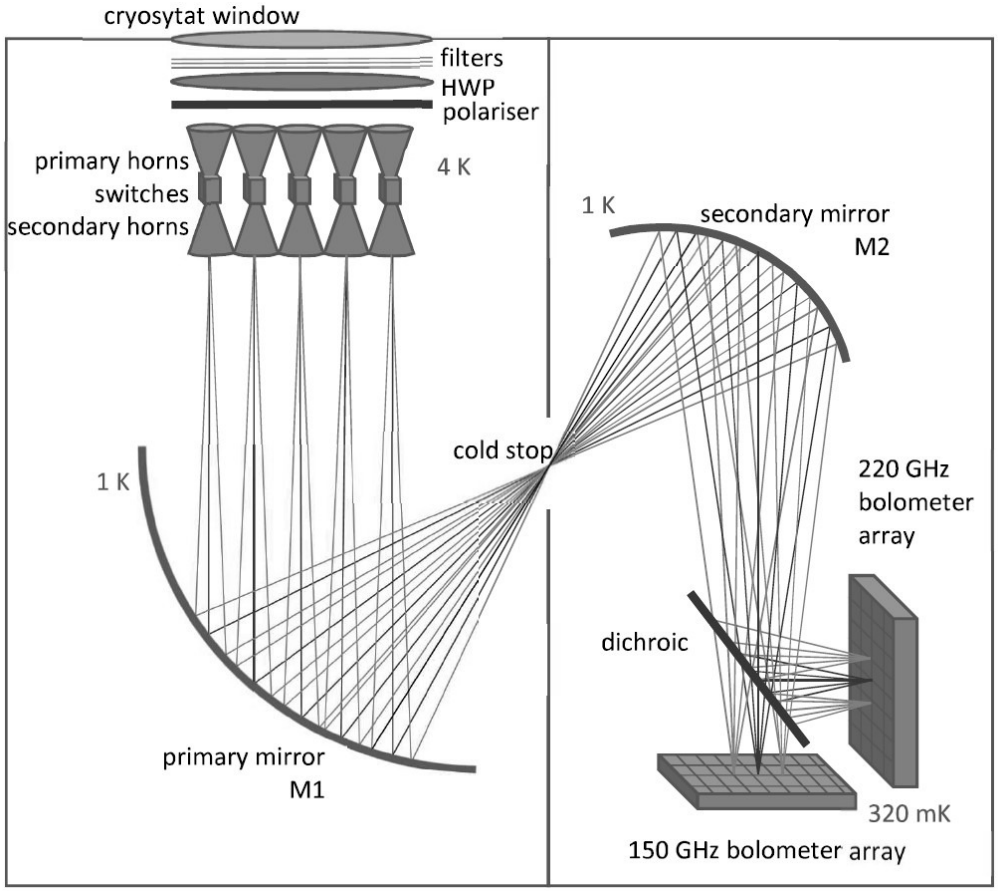

Figure 2. Schematic diagram of the QUBIC instrument.

The signal from the sky enters the cryostat through a window and series of filters. If we write the incoming radiation in terms of its electric field in orthogonal directions, E_x and E_y, then after the half-wave plate the signal in those directions will be

$$S_{HWP} = \begin{pmatrix} E_x \cos 2\phi(t) + E_y \sin 2\phi(t) \\ E_x \sin 2\phi(t) - E_y \cos 2\phi(t) \end{pmatrix}$$

where $\phi(t)$ is the time-varying angle of rotation of the waveplate. The polarising grid then removes the signal in one direction giving

$$S = \begin{pmatrix} E_x \cos 2\phi(t) + E_y \sin 2\phi(t) \\ 0 \end{pmatrix}$$

or, in terms of the Stokes' parameters[5,10], $S = I + Q\cos 4\phi(t) + U\sin 4\phi(t)$. This signal is coupled to the open sky-facing primary horns and then re-emitted by the secondary horns into the cold (1 K) beam combiner and imaged onto a focal plane (320 mK). The focal-plane detectors are not sensitive to polarisation and so measure the signal, S, which is unchanged by any cross-polarisation after the polariser. The modulation of the signal as a function of HWP angle $\phi(t)$ allows I, Q and U to be reconstructed. A dichroic filter splits the signals into two frequency bands that are imaged simultaneously on orthogonal focal planes as illustrated in Figure 2.

Typically, in interferometry, the signal from individual baselines (pairs of back-to-back horn combinations in our case) are measured but QUBIC will be used as a synthetic imager, observing the fringes from all baselines simultaneously (the switches in all back-to-back horns will be open). This combined fringe pattern is simply an image of the sky (in I, Q and

Downloaded From: https://www.spiedigitallibrary.org/conference-proceedings-of-spie on 12/20/2018
Terms of Use: https://www.spiedigitallibrary.org/terms-of-use

U as explained above) convolved with the synthesised beam of the instrument. The advantage of this, over traditional imaging, is that since equivalent baselines produce identical fringe patterns we can exploit the redundancy of baselines in a calibration technique that offers unprecedented control of systematics[7,8]. On the other hand, imaging the fringes with a bolometer array gives us a sensitivity comparable to that of more traditional imaging polarimeters. In addition, a bolometric interferometer such as QUBIC is in fact a synthesized spectro-imager, allowing sky maps to be produced at multiple sub-frequencies with data acquired by bolometers operating over a single wide bandwidth.

Figure 3 shows the fringe pattern on a focal plane (for an ideal combiner) for a selection of baselines observing an on-axis point source in the sky. Figure 3(e) shows the image when all baselines are included. The equivalent synthetic beam on the sky has an on-axis peak of width ~0.5° (determined by the horn array size) and subsidiary maxima 8.5° away (determined by the horn array spacing). The field-of-view of the instrument and the relative heights of the main and subsidiary peaks are determined by the 13° FWHM horn beam patterns. The map-making procedure is necessarily more complex for such an instrument compared with a standard imager[5,10].

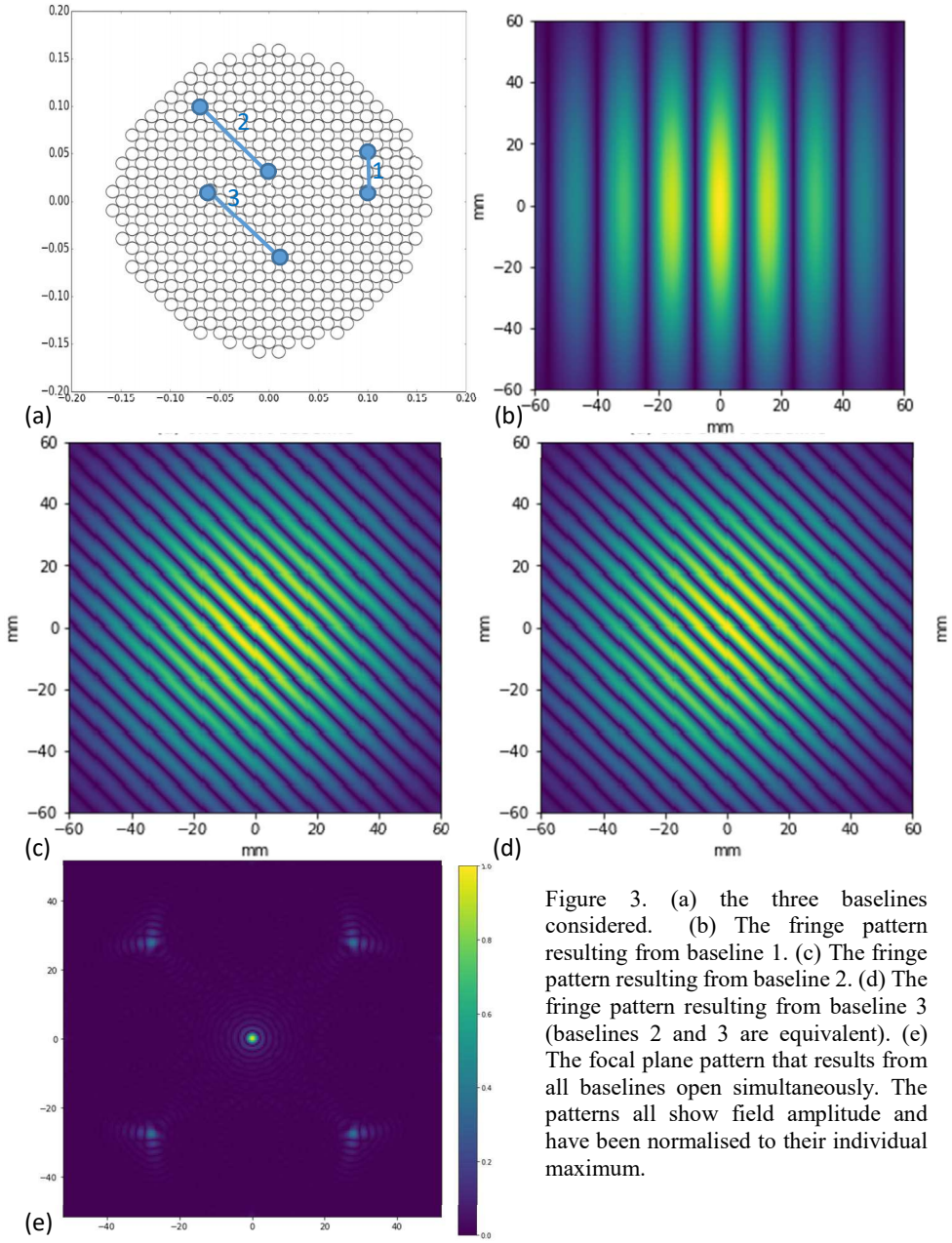

Figure 3. (a) the three baselines considered. (b) The fringe pattern resulting from baseline 1. (c) The fringe pattern resulting from baseline 2. (d) The fringe pattern resulting from baseline 3 (baselines 2 and 3 are equivalent). (e) The focal plane pattern that results from all baselines open simultaneously. The patterns all show field amplitude and have been normalised to their individual maximum.

Downloaded From: https://www.spiedigitallibrary.org/conference-proceedings-of-spie on 12/20/2018
Terms of Use: https://www.spiedigitallibrary.org/terms-of-use

3. THE QUBIC INSTRUMENT

3.1 The Cryostat

The QUBIC cryostat (Figure 4(a)) houses the full optical chain and so is extremely large, having a diameter of 1.4 m and a height of 1.5 m. Two 1-W pulse tube cryocoolers work in parallel to cool the main instrument volume to 4 K and the surrounding radiation shield to 40 K. A superinsulation blanket is placed between the outer shell and the 40K shield to reduce the radiative load. The 4 K stage includes the half-wave plate (HWP), polarising grid, back-to-back horns and switches. A 1 K box (Figure 4(b)) with the combiner mirrors, the dichroic and part of the readout electeonics is suspended from the 4 K stage and cooled by a high capacity 4He closed-cycle sorption cooler. Mounted from the 1 K box is the 320 mK stage for the focal plane arrays and this is cooled by a double stage 4He/3He sorption cooler (Chase Cryogenics). The design, analysis and testing of such a large and complex cryostat was challenging and is described in more detail in May et al. (2018)[11].

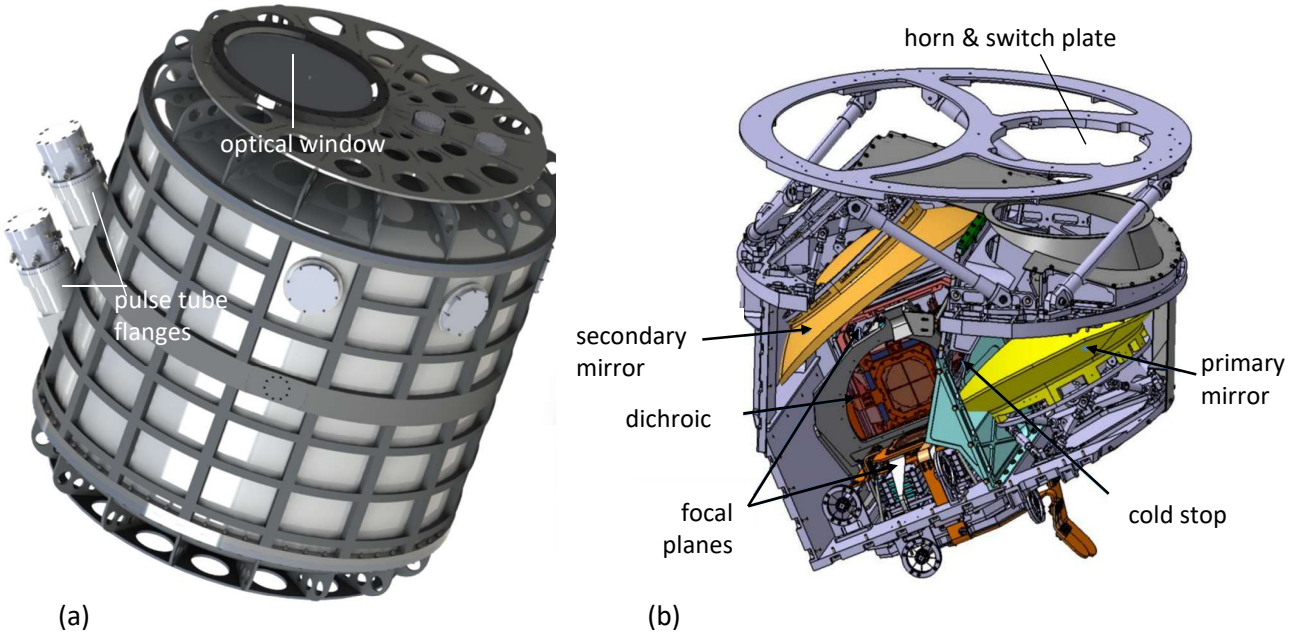

Figure 4. (a) The cryostat outer shell. The large (~40-cm) UHMW PE optical window (Section 3.2) can be seen at the top. The pulse tubes are tilted at 40° to the cryostat vertical so that during observations the pulse tube heads can be maintained close to vertical for optimum performance. (b) The cryostat 1 K box.

3.2 Quasi-Optical Components (HWP, Polariser Filters and Dichroic)

Window

The cryostat window is made from a cylindrical section (20 mm thick) of ultra high molecular weight polyethylene (UHMW PE)[12]. UHMW PE was chosen as the best compromise between transparency at millimetre waves and the stiffness required to withstand the large force from atmospheric pressure. The window is pressed against the top cover of the cryostat by an aluminium ring.

HWP and Polariser

In QUBIC, polarisation modulation is achieved by rotating a HWP (Figure 5) in front of the sky-facing horns. The required clear diameter is 300 mm and it must exhibit achromatic behaviour across the two QUBIC frequency bands, i.e. a relative

Downloaded From: https://www.spiedigitallibrary.org/conference-proceedings-of-spie on 12/20/2018
Terms of Use: https://www.spiedigitallibrary.org/terms-of-use

bandwidth on the order of 73%. This is achieved using a metamaterial developed using embedded mesh technology [13]. The QUBIC design is based on 12 anisotropic mesh grids giving an overall thickness of the order of 3.5 mm. Tests show that the expected performance of the QUBIC mesh is an average transmission of 98%, absorption <1% and cross-polarisation of ~-20dB[6].

Since the HWP is mounted on the 4 K stage of the cryostat, a cryogenic rotation mechanism is needed. We use a stepper motor mounted outside the cryostat shell that can position the HWP in 7 different positions, 15° apart, for redundant coverage of the position angles that are needed. Motion is transmitted through the shell by means of a magnetic joint.

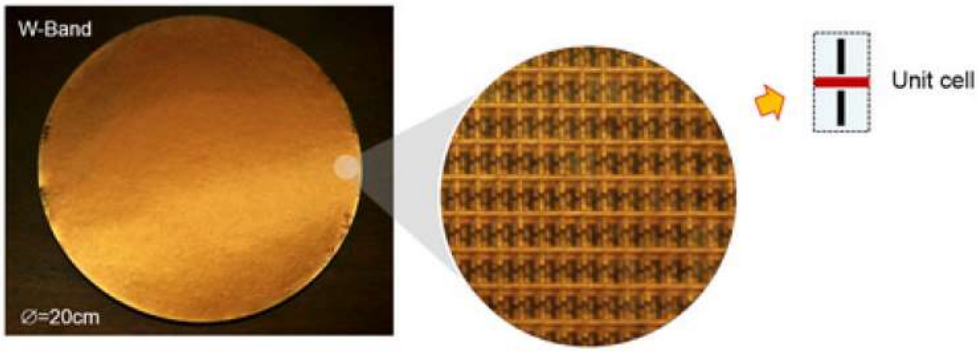

Figure 5. Embedded mesh HWP based on metamaterials. (Taken from Pisano et al.[14]).

A 10 μm period photolithographic wired polariser is used to select a single polarisation following the HWP. A 450-mm prototype suitable for operation at 4 K has already been manufactured.

Filters

In QUBIC, quasi-optical filters are used for two purposes: blocking out-of-band radiation to reduce thermal loading and defining the required band edges of the 150- and 220-GHz channels (25% bandwidth).

The cryostat window itself already acts as a filter by reflecting and absorbing most of the short wavelength radiation up to the near-infrared. Between the window and the sky-facing horns are a series of single-layer metal-mesh thermal (IR) and low-pass blocking filters[13], carefully designed to have minimal impact on the instrument beam pattern. Filters designed to block out-of-band FIR radiation are also located at thermal stage apertures after the back-to-back horns but these, coming after the polarisation modulation, have less impact on the instrument systematics. The details of filter sizes and locations can be found in the QUBIC Technical Design document[6].

The definition of the two QUBIC spectral bands is achieved using a combination of the horn waveguide section (for the frequency cut-on of 150-GHz band) and metal-mesh interference filters (for the 150-GHz cut-off and the 220-GHz band). The spectral band defining filters are located close the detectors at the aperture of the 320 mK stage.

Dichroic

The dichroic filter will be used for frequency selection immediately before the QUBIC foal planes. It is designed to transmit (>90%) the 150-GHz band, whilst reflecting (>90%) the 220-GHz band. Prototype hot-press and air-gap HPE devices have been produced by and shown to be effective in both reflection and transmission[6]. Development is ongoing on a device that is sufficiently large for QUBIC and that can operate at a range of incident angles.

The design and manufacture of quasi-optical components (mesh filters, HWP, polariser and dichroic) that are sufficiently large not to degrade the horn beams and yet can maintain their flatness, have low induced instrumental polarisation and

Downloaded From: https://www.spiedigitallibrary.org/conference-proceedings-of-spie on 12/20/2018
Terms of Use: https://www.spiedigitallibrary.org/terms-of-use

withstand cryogenic cycling is challenging. The QUBIC components are being manufactured by the Astronomy Instrumentation Group of Cardiff University.

3.3 Horns and Switches

QUBIC observes the sky through a 400-element array of back-to-back horns at the entrance aperture. The horns are arranged as shown in Figure 6(a). The signals are re-emitted from the downward facing horn of each pair and are combined quasi-optically. A movable shutter placed in the middle of each back-to-back pair acts as an RF switch so that individual baselines can be selected during self-calibration.

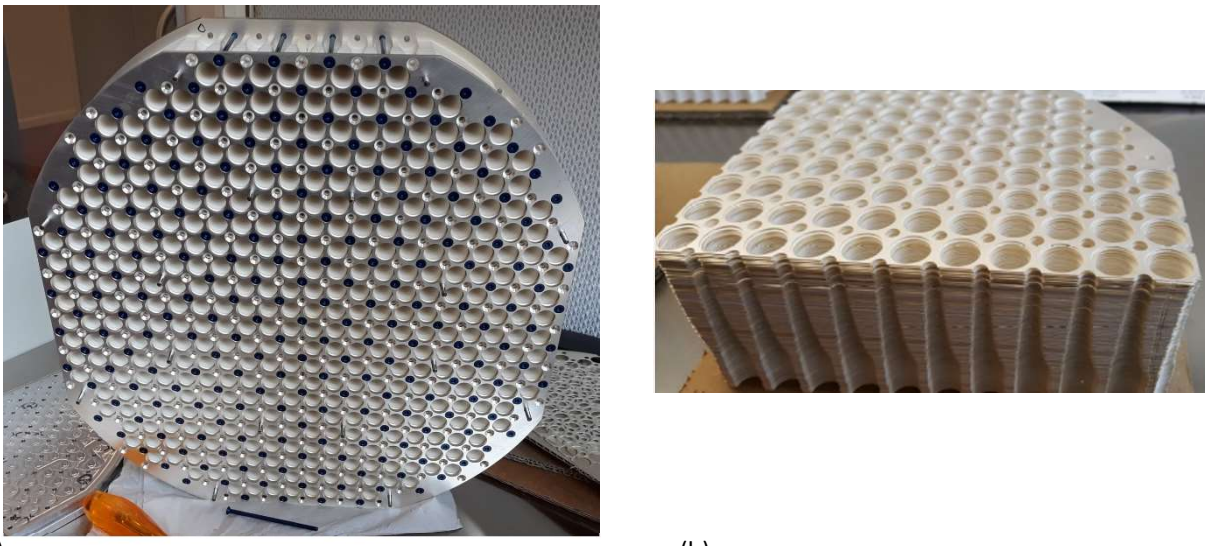

(a) (b)

Figure 6. (a) The top flange showing the layout of the 400-element input horn array. (b) Photograph of one quarter of the platelet horns (one element of each back-to-back pair).

Each feed is a corrugated horn that has been optimised to operate in both QUBIC frequency bands simultaneously (i.e. in the range 130 – 240 GHz). In the lower frequency band the horns are single-moded (transmit only the HE_{11} mode) whereas in the upper band three modes can propagate (HE_{11}, E_{02}, EH_{21})[15]. The HE_{11} and EH_{21} modes also have orthogonal modes that are transmitted. The horn behaviour at specific frequencies was modelled using the electromagnetic mode-matching technique[16] (Figure 7). At 150 GHz the beam is highly Gaussian with a FWHM of 12.9°. The beam pattern in the upper-band is narrower.

The horn array has been manufactured using a platelet technique where holes are chemically etched into aluminium plates (Figure 6(b)). In our case the array is made in four quarters, each one consisting of 176 0.3-mm thick platelets, corresponding to the 88 corrugations of the horn design. The four quarters are held together by two 3-mm thick flanges (top and bottom) directly milled from solid aluminium. One flange contains the 400 horn apertures while the opposite one contains the throats which are interfaced to the switch block. The whole block is mechanically clamped using ERGAL screws. The sky-facing and re-emitting horns are made separately so eight such quadrants make up the full back-to-back array. The centres and radii of a subset of QUBIC horns have been measured and, with very few exceptions, they reach the mechanical tolerance of 0.05 mm that we specified. Our simulations, which agree well with laboratory measurements, show that the beam patterns from the horns, as manufactured, behave well, even at the highest QUBIC frequencies[17].

The switches are single pole single throw (SPST) and operate by means of a blade (shutter) blocking the circular waveguide between the back to back horns. The blade is activated by an electromagnet pushing and pulling a ferrite soldered to a hook connected to the shutter. The switches have been designed to have good return loss, low insertion loss, low instrumental polarisation, and to work reliably at 4 K[6].

Downloaded From: https://www.spiedigitallibrary.org/conference-proceedings-of-spie on 12/20/2018
Terms of Use: https://www.spiedigitallibrary.org/terms-of-use

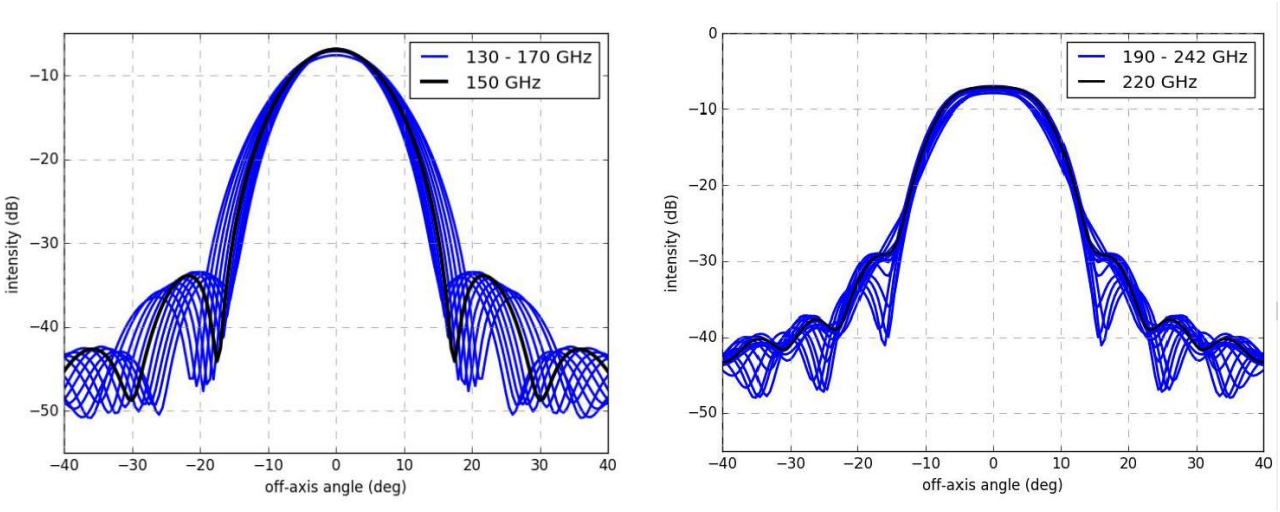

Figure 7. (Left) Farfield beam patterns calculated across the 150 GH band (4-GHz intervals) where the horns are single-moded and (right) the beam patterns across the 220-GHz band in 4-GHz intervals (taken from Burke et al.[17]).

3.4 The Optical Combiner

The optical combiner is an imager that superimposes the beams from the downward facing horns on two focal planes. It has a compensated off-axis Gregorian design that also obeys the Rusch condition for minimum spillover[18]. The requirement to sample the narrowest fringes (the longest baselines of interest) with two or more 3-mm wide detectors limits the focal length to 300 mm. This short focal length means that aberrations are an issue, but our simulations have shown that they nevertheless only decrease the sensitivity of the instrument by about 6%[19]. The use of reflectors means that the system can be accurately modelled with physical optics (PO) software such as GRASP[20].

The layout of the combiner in the cryostat 1 K box is shown in Figure 8. The primary mirror (M1) is close to parabolic and the secondary (M2) is elliptical. Each is supported on a hexapod allowing six degrees of freedom for alignment. A cold shield is placed around the focal planes and secondary mirror to reduce background loading on the bare array of detector bolometers (see Section 3.5). There is no accessible intermediate aperture stop in the system and we refer to the cold shield aperture as the cold stop. A dichroic transmits the 150-GHz signal onto the on-axis focal plane while simultaneously reflecting the 220-GHz signal to the orthogonal off-axis focal plane. An optical shield around the dichroic eliminates direct radiation from the horns below 16° and we expect any remaining stray light to be negligible compared with our signal. The component sizes were determined after a full PO analysis of all 400 beams propagating through the combiner[21]. The most stringent criteria come from the 150-GHz beams as they are wider than at 220 GHz.

Two carbon-fibre illuminators[22] will be installed on the edges of the horn and switch plate for use in cold optical alignment cross-checks as well as for monitoring the inter-calibration of the TES detectors.

3.5 Detection Chain

As described in Section 2, the QUBIC instrument has two focal planes: an on-axis focal plane operating at 150 GHz and an off-axis one at 220 GHz. Each is composed of four 256-pixel arrays combined to give a 1024-pixel, approximately circular, detector (Figure 9(a)) . The pixels are spaced at 3-mm resulting in an overall focal-plane radius of ~51 mm. Each pixel consists of a superconducting Transition Edge Sensor (TES) biased to operate in the narrow temperature range where it transitions from the normal to superconducting state. A small increase in temperature can therefore cause a dramatic change in resistance, making these very sensitive bolometers. The TES readouts are time-domain multiplexed using SQUID current amplifiers. The total noise equivalent power (NEP) of the devices is of the order of 4×10^{-17} W$/\sqrt{\text{Hz}}$ at 150 GHz, and they have a time constant in the 10-100 ms range. The TES bolometers are not intrinsically sensitive to polarisation.

Downloaded From: https://www.spiedigitallibrary.org/conference-proceedings-of-spie on 12/20/2018
Terms of Use: https://www.spiedigitallibrary.org/terms-of-use

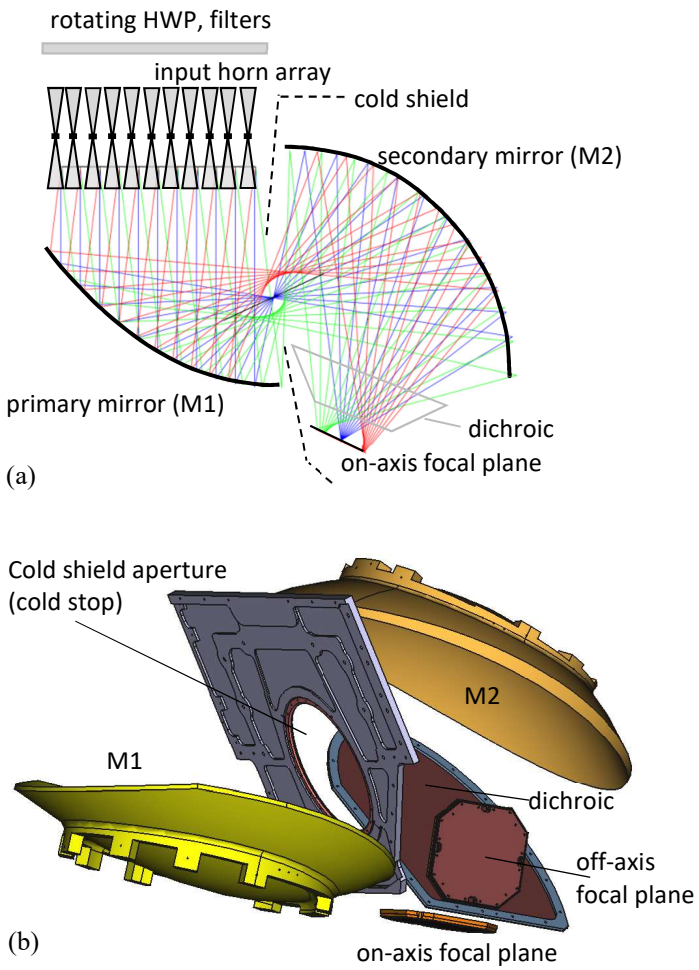

Figure 8. Layour of the QUBIC optical beam combiner. (a) and (b) show the layout of the main components, some additional electronics and supporting structure are shown in (c).

The detection chain for each pixel is shown in Figure 9(b) and consists of five main parts: the TES detector, the TES voltage biasing and SQUID (StarCryoelectronics[23]) multiplexer, the cold low-noise amplifier (LNA ASIC) the warm LNA and digital readout. Light absorption is via a metallic (Pd) grid (2.7×2.7 mm^2) in a quarter-wave cavity and the TES sensors themselves are made with a Nb_xSi_{1-x} amorphous thin film ($x \approx 0.15$) and Al comb electrodes. The TESs are voltage biased ($V_{TES} = R_{sh} \times I_{bias}$) so that they operate in the extreme electro-thermal feedback mode giving increased bandwidth, direct power calibration and self-regulation of the TESs at their normal-to-superconducting transition temperature (320 mK). The critical temperature is increased for the 220-GHz TESs due to the higher saturation power required for multi-mode operation.

Downloaded From: https://www.spiedigitallibrary.org/conference-proceedings-of-spie on 12/20/2018
Terms of Use: https://www.spiedigitallibrary.org/terms-of-use

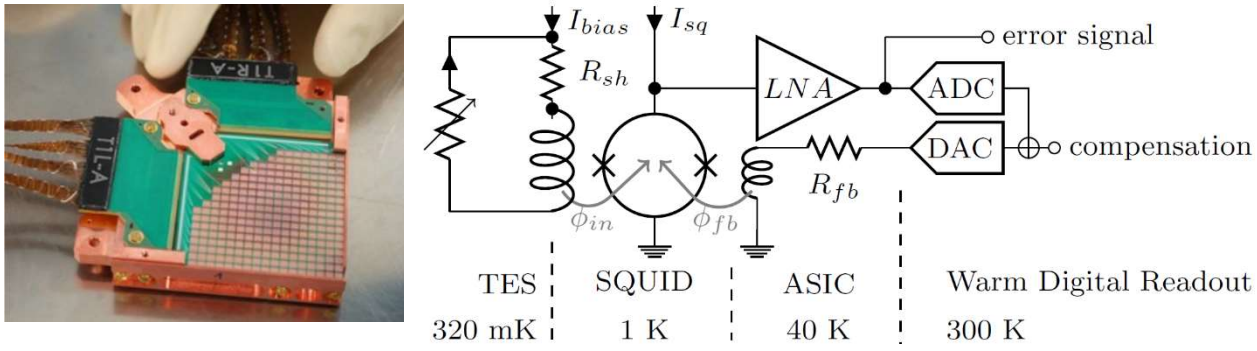

Figure 9. (a) A 256-pixal array of TESs (quarter focal plane) being integrated for test[6] and (b) the QUBIC detection chain[6].

A 4-to-1 multiplexed LNA sequentially reads out 4 columns of 32 multiplexed SQUIDS and each of these 128 TESs are managed by a single ASIC operated at a cryogenic temperature. A total of 16 ASICs are therefore required for the 2 full focal planes. The room temperature readout electronics are designed to control and adjust the operating biasing and feedback to TESs and their associated SQUIDs. They read out the signal from the cold multiplexing ASIC and send compressed scientific data to the data acquisition system. Custom software synchronises and manages the readout and detector operation sampling the TESs at a frequency of up to 200kHz. The experimental characterisation of the QUBIC TES arrays and their multiplexing readout chain is described in detail in another paper[24].

A single interface, we have called 'QUBIC Studio', has been designed by researchers in IRAP to deal with the readout, the control command software and the data storage.

3.6 Mount and Baffles

The QUBIC mount (Figure 10(a)) is a classical alt-az astronomical mount with additional rotation about the instrument optical axis. Pointing accuracy will be better than 15″ in elevation and azimuth and 5′ about the instrument axis. The speed about all axes will be adjustable between 0 and 5 °s^{-1} with a maximum acceleration of 10 °s^{-2}.

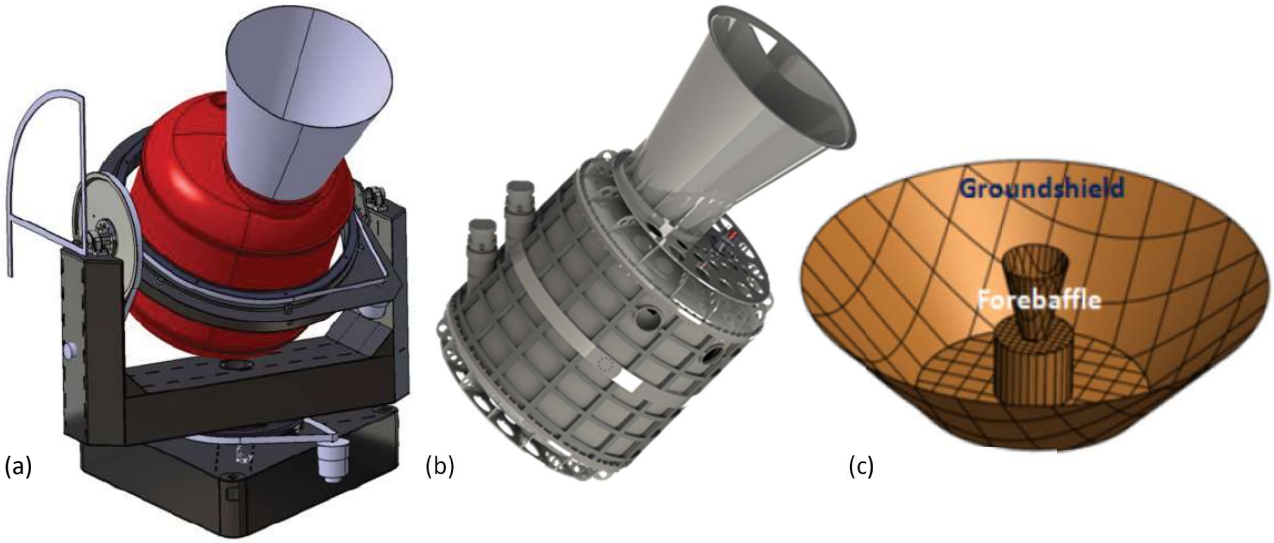

Figure 10. (a) A drawing of the QUBIC outer structure and mount, atop a platform, showing the forebaffle cone around the cryostat window[6]. (b) The QUBIC cryostat and forebaffle. (c) A plot of the QUBIC groundshield and forebaffle used in optical simulations[6].

Downloaded From: https://www.spiedigitallibrary.org/conference-proceedings-of-spie on 12/20/2018
Terms of Use: https://www.spiedigitallibrary.org/terms-of-use

A ground shield and forebaffle (Figure10(b),(c)) will be used to shield the QUBIC instrument from stray radiation. The reflective ground shield will be manufactured with several flat panels (petals) to fit an overall conical shape with a base of 3 m in diameter, a flared aperture of 5 m in diameter and cone angle of 45°. The forebaffle, on the other hand, will be manufactured as a single conical structure (angle ~50°, base and aperture diameter of approximately 0.35 m and 0.85 m, respectively) with a dismountable flare.

Both will be manufactured with an aluminium alloy but the forebaffle will be absorptive having its inner surface covered with an Eccosorb dielectric layer. Detector loading due to forebaffle emission is expected to be negligible when compared with atmospheric emission. The groundshield will be fixed on the same platform as the mount and so will not move with the instrument. The forebaffle will be fixed around the cryostat window (Figure 10(b)) and will move along with it. The spillover contributions from the main contaminants, with and without the presence of the shields, are listed in Table 1.

Table 1 Main spillover contributions in terms of brightness temperature[6].

At zenith	no shields	foreground baffle only	foreground baffle + groundshield
Ground	627 mK	117 mK	2mK
Sun	3 mK	328 μK	7 μK
Moon	70 μK	7 μK	0.1 μK

3.7 The QUBIC site

The first QUBIC module will be installed in Argentina, near the city of San Antonio de los Cobres, Salta Province , at the Alto Chorillos site (Figure 11(a)), close to the LLAMA telescope[25]. The site has coordinates 24° 11′ 11.7″ S; 66° 28′ 40.8″ W and is at an altitude of 4869 m above sea level. It is located about 180 km from the Chajnantor site where other millimetre-wave experiments (ALMA[26], ACTPol[27], PolarBear[28]) are located and has similar atmospheric properties. Temperature, humidity and wind speed have been monitored on site for several years and, except during the summer (December to March period), it is suitable for CMB observations.

The target fields for QUBIC are visible from the site (above 30°and below 70° elevation) for about 40% of the time. However, self-calibration can be performed during the periods when a target is not visible. Simulations (Figure 11(b)) have shown that, if we spend 12 hours per day doing self-calibration, the sensitivity achievable from Argentina is reduced by a factor of about 1.4 compared with the Dome C site in Antarctica that was originally proposed.

4. THE QUBIC TECHNICAL DEMONSTRATOR

As a step towards the first full QUBIC module, it was decided to build a QUBIC technological demonstrator (TD) to validate the QUBIC design and test it electrically, thermally and optically. The TD differs from the full instrument in that it has a reduced number of detector pixels (256 pixels i.e. one quarter of one focal plane), a reduced number of horns and switches (the central 8×8 horns of the array), reduced primary and secondary mirror size (400 mm in diameter rather than 600 mm) reduced filter sizes (up to 280 mm in diameter) and a neutral density filter instead of a dichroic. The scaling-down of the instrument for the demonstrator means that the mirrors, switches and horn array could be manufactured in-house (University of Milan, University of Milano Bicocca).

A calibration plan[29] has been drawn up that aims to characterise the instrument performance with the minimum number of cryostat cool-downs. Three types of source will be used: the two carbon-fibre sources mounted beside the input horn array will be used for alignment checks and for relative calibration of the TES pixels, a far-field Gaussian source will be used to test the autocalibration technique and for synthesised beam reconstruction, and a full-beam polarised source[30] will be used to provide absolute polarisation calibration. The TD is currently undergoing integration, testing and calibration at the Laboratoire Astroparticule & Cosmologie (APC) in Paris before deployment of the first module in Argentina.

Downloaded From: https://www.spiedigitallibrary.org/conference-proceedings-of-spie on 12/20/2018
Terms of Use: https://www.spiedigitallibrary.org/terms-of-use

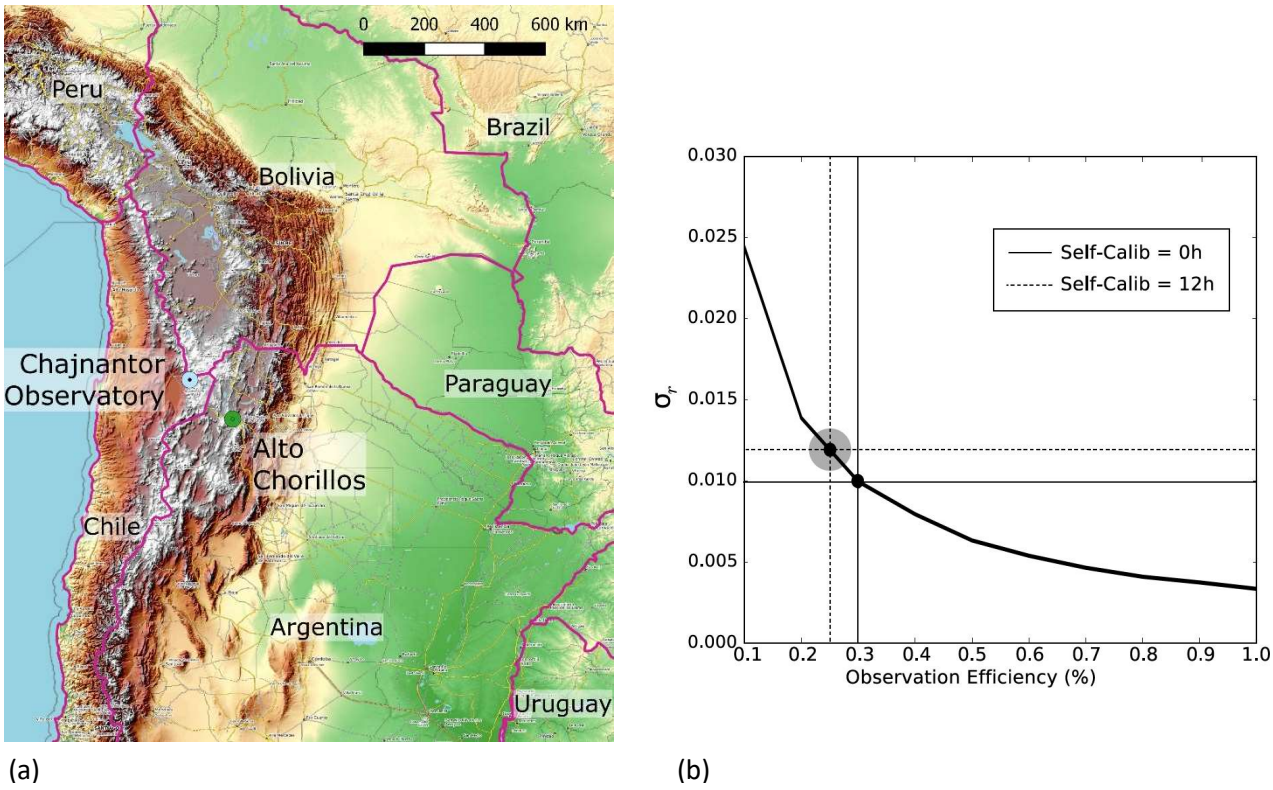

Figure 11. (a) The Alto Chorrillos site in Argentina (© OpenStreetMap contributors). (b) An assessment of the site quality in Alto Chorrillos for QUBIC in terms of $\sigma(r)$. The circle corresponds to the case in which 12 hours a day are spent in self-calibration mode (Taken from Menella et al.[9]).

5. SUMMARY

In this paper we have described the QUBIC instrument that aims to measure the CMB B-modes using the technique of bolometric interferometry. We have introduced the concept behind the operation of QUBIC as well as describing its different subsystems, site and scientific aims. A QUBIC technological demonstrator is currently undergoing test and calibration in France.

ACKNOWLEDGEMENTS

INFN in Italy and IN2P3/CNRS in France are thanked for their funding of the QUBIC project. D. Burke and J.D. Murphy acknowledge funding from the Irish Research Council under the Government of Ireland Postgraduate Scholarship scheme. M. De Leo thanks the Astrophysics Group at the University of Surrey for allowing his continued participation in the QUBIC Collaboration.

REFERENCES

[1] Bond, J.R., and Efstathiou, G., "The statistics of cosmic background radiation fluctuations", MNRAS, 226, 655 (1987).
[2] Planck Collaboration: Adam, R., et al., "Planck 2015 results I. Overview of products and scientific results", Astronomy & Astrophysics, Volume 594, id.A1, pp.38 (2016).

Downloaded From: https://www.spiedigitallibrary.org/conference-proceedings-of-spie on 12/20/2018
Terms of Use: https://www.spiedigitallibrary.org/terms-of-use

[3] Zaldarriaga, M. & Seljak, U., “An all-sky analysis of polarization in the microwave background”, Phys. Rev. D, 55, p.1830 (1997).
[4] Keck Array and BICEP2 Collaborations: Ade, P.A.R., et al., “Improved constraints on cosmology and foregrounds from BICEP2 and Keck Array cosmic microwave background data with inclusion of 95 GHz Band”, Phys. Rev. Lett. 116, 031302 (2016).
[5] Battistelli, E., et al., “QUBIC: The QU bolometric interferometer for cosmology”, Astroparticle Physics 34, 705–716 (2011).
[6] The QUBIC Collaboration, Aumont, J., et al.,“QUBIC Technical Design Report”, arXiv:1609.04372v2 (2016).
[7] Bigot-Sazy, M.-A.,et al., “Self-calibration : an efficient method to control systematic effects in bolometric interferometry”, Astron. & Astrophys.,550, A59 (2013).
[8] Charlassier, R., et al., “An efficient phaseshifting scheme for bolometric additive interferometry”, Astron. & Astrophys., 497, 963–971 (2009).
[9] Mennella, A., et al., “QUBIC - The Q&U Bolometric Interferometer for Cosmology - A novel way to look at the polarized Cosmic Microwave Background”, Proc. EPS Conference on High Energy Physics, Venice, Italy (2017).
[10] Stolpovskiy, M., “Development of the B-mode measurements pipeline foe RUBIC experiment”, PhD Thesis, Université Paris Diderot, Paris-7 (2016).
[11] May, A., et al., “Thermal architecture for the QUBIC cryogenic receiver”, these proceedings.
[12] D'Alessandro, G., et al., “Ultra high molecular weight polyethylene: optical features at millimeter wavelengths”, Infrared Physics and Technology, Vol. 90, pp. 59-65 (2018).
[13] Ade, P.A.R., et al., “A Review of Metal Mesh Filters”, Proc. of SPIE Vol. 6275, Millimeter and Submillimeter Detectors and Instrumentation for Astronomy III, 62750U, (2006).
[14] Pisano G. et al., “A Broadband Metal-Mesh Half-Wave Plate for Millimetre Wave Linear Polarisation Rotation”, PIER M, 25, 101-114, (2012).
[15] Scully, S., “Quasi-Optical Design and Analysis of a Bolometric Interferometer for Cosmic Microwave Background Experiments”, PhD Thesis, National University of Ireland, Maynooth (2016).
[16] Murphy, J. A., et al., “Radiation patterns of multi-moded corrugated horns for far-IR space applications”, Infrared Phys. and Tech., 42, 515-528 (2001).
[17] Burke, D., et al., "Optical modelling and analysis of the Q and U bolometric interferometer for cosmology", Proc SPIE Photonics West, San Francisco, USA, (to be published 2018).
[18] Rusch W. V. T., et al., "Derivation and application of the equivalent paraboloid for classical offset Cassegrain and Gregorian antennas", IEEE Trans. Antennas and Propagat. 38, (8), 1141 (1990).
[19] O’Sullivan, C., et al., “Simulations and performance of the QUBIC optical beam combiner”, these proceedings.
[20] GRASP10, TICRA Engineering Consultants. Online http://www.ticra.com/software/grasp/ (May 2018).
[21] Gayer, D., et al.,“FreeCAD visualization of realistic 3D physical optics beams within a CAD system-model”, Proc. SPIE, Vol. 9914, id. 99142Y 14 pp. (2016).
[22] Henrot-Versillé, S., et al., “Pulsed Carbon fiber illuminators for FIR instrument characterization”, Infrared Physics &Technology, 52 159,165 (2009).
[23] Star Cryoelectronics, https://starcryo.com/ (May2018).
[24] Salatino, M., et al., "Performance of NbSi Transition Edge Sensors read out with a 128 MUX factor for the QUBIC experiment", these proceedings.
[25] Lepine, J., et al., “The LLAMA 12 m mm/sub-mm radiotelescope in the Andes”, IAU General Assembly 22, 2247050 (2015).
[26] Brown, R.L., et al. “ALMA - the Atacama large millimeter array”, Advances in Space Research, Volume 34, Issue 3, p. 555-559 (2004).
[27] Thornton, R.J., et al., “ The Atacama technology Telescope: The polarization-sensitive ACTPol instrument”, ApJ. Suppl. Series, 227, 21 (2016).
[28] Inouea, Y. Et al., “POLARBEAR-2: an instrument for CMB polarization measurements”, Proc. SPIE, Vol. 9914, id. 99141I (2016).
[29] Henrot-Versillé, S., et al., “QUBIC Calibration plans”, QUBIC internal note (2018).
[30] Puddhu, R., "A full-beam calibrator for the QUBIC experiment and site testing in the Antarctic plateau", PhD Thesis, Università di Siena (2016).

Downloaded From: https://www.spiedigitallibrary.org/conference-proceedings-of-spie on 12/20/2018
Terms of Use: https://www.spiedigitallibrary.org/terms-of-use